A hydrodynamic model for Galveston Bay and the shelf in the northern Gulf of Mexico

Jiabi Du[1], Kyeong Park[1], Jian Shen[2], Yinglong J. Zhang[2], Xin Yu[2], Fei Ye[2], Zhengui Wang[3], Nancy N. Rabalais[4]

[1]Department of Marine Sciences, Texas A&M University at Galveston, Galveston, TX 7754, USA

[2]Virginia Institute of Marine Science, College of William and Mary, Gloucester, VA 23062, USA

[3]School of Marine Sciences, University of Maine, Orono, ME 04469, USA

[4]Louisiana State University, Baton Rouge, LA 70803, USA

Correspondence to: Jiabi Du (jdu@tamug.edu)

Abstract: A 3D unstructured-grid hydrodynamic model for the northern Gulf of Mexico was developed, with a hybrid s-z vertical grid and high-resolution horizontal grid for the main estuarine systems along the Texas-Louisiana coast. This model, based on the Semi-implicit Cross-scale Hydroscience Integrated System Model (SCHISM), is driven by the observed river discharge, reanalysis atmospheric forcing, and open boundary conditions from global HYCOM output. The model reproduces well the temporal and spatial variation of observed water level, salinity, temperature, and current velocity in Galveston Bay and on the shelf. The validated model was applied to examine the remote influence from neighboring large rivers, specifically the Mississippi-Atchafalaya River (MAR) system, on the salinity, stratification, vertical mixing, and longshore transport along the Texas coast. Numerical experiments reveal that the MAR discharge could significantly decrease the salinity and change the stratification and vertical mixing on the inner Texas shelf. It would take about 25 and 50 days for the MAR discharge to reach the mouth of Galveston Bay and Port Aransas, respectively. Influence of the MAR discharge is sensitive to the wind field. Winter wind constrains the MAR freshwater to form a narrow lower-salinity band against the shore from the Mississippi Delta all the way to the southwestern Texas coast, while summer wind reduces the downcoast longshore transport significantly, weakening the influence of the MAR discharge on surface salinity along Texas coast. However, summer wind causes a much stronger stratification on the Texas shelf, leading to a weaker vertical mixing. The decrease in salinity of up to 10 psu at the mouth of Galveston Bay due to the MAR discharge results in a decrease in horizontal density gradient, a

decrease in the salt flux, a weakened estuarine circulation and estuarine-ocean exchange. We highlight the flexibility of the model and its capability to simulate not only estuarine dynamics and shelf-wide transport but also the interactions between them.

1. Introduction

Northern Gulf of Mexico (GoM) is characterized by complicated shelf and coastal processes including multiple river plumes with varying spatial scales, highly energetic deep-current due to steep slopes, upwelling in response to alongshore wind, and mesoscale eddies derived from Loop Currents of Gulf Stream (Oey et al., 2005; Dukhovskoy et al., 2009; Dzwonkowski et al., 2015; Barkan et al., 2017). Freshwater from the Mississippi-Atchafalaya River (MAR) basin introduces excess nutrients and terminates amidst one of the United States' most productive fishery regions and the location of the largest zone of hypoxia in the western Atlantic Ocean (Rabalais et al., 1996, 2002; Bianchi et al., 2010). The physical, biological, and ecological processes in the region have been attracting increasing attention, given its sensitive response to large-scale climate variation, accelerated sea-level rise, and extensive anthropogenic interventions (Justić et al., 1996; Rabalais et al. 2007).

Understanding the interaction and coupling between regional scale ocean dynamics and local scale estuarine processes is of great interest. Many observational (in-situ/satellite) (e.g., Cochrane and Kelly, 1986; DiMarco et al., 2000; Chu et al., 2005) and numerical modeling (e.g., Zavala-Hidalgo et al., 2003, 2006; Hetland and Dimarco, 2008; Fennel et al., 2011; Gierach et al., 2013; Huang et al., 2013) studies have been conducted for the shelf of GoM. Hetland and Dimarco (2008) configured a hydrodynamic model based on the Regional Ocean Modelling System (ROMS: Shchepetkin and McWilliams, 2005) for the Texas-Louisiana shelf, which has been used for the subsequent physical and/or biological studies (Fennel et al., 2011; Laurent et al., 2012; Rong et al., 2014). Zhang et al. (2012) extended the model domain westward to cover the entire Texas coast. Wang and Justić (2009) applied the Finite Volume Coast Ocean Model (FVCOM: Chen et al., 2006) over the similar domain of Hetland and Dimarco (2008). Lehrter et al. (2013) applied the Navy Coastal Ocean Model (NCOM: Martin, 2000) over the inner Louisiana shelf with focus on the Mississippi River plumes. In addition, there were modeling studies for larger domains such as the entire GoM (Oey and Lee, 2002; Wang et al., 2003; Zavala-Hidalgo et al., 2003). For example, Zavala-Hidalgo (2003) used the NCOM to investigate

the seasonally varying shelf circulation in the western shelf of the GoM. Bracco et al. (2016) used the ROMS to examine the mesoscale and sub-mesoscale circulation in the northern GoM.

60   Other hydrodynamic modeling studies focused on specific estuarine systems such as Galveston Bay (Rayson et al., 2015; Rego and Li, 2010; Sebastian et al., 2014), Mobile Bay (Kim and Park, 2012; Du et al., 2018a), and Choctawhatchee Bay (Kuitenbrouwer et al., 2018). These models tend to have smaller domains, including the target estuary and the inner shelf just outside of the estuary. The dynamics in these coastal bays are affected by both the large-scale shelf conditions and localized small-

65   scale geometric and bathymetric features such as narrow but deep ship channels, seaward extending jetties, and offshore sandbars, which are typically on the order of 10 to 100 m. Including both the estuarine and shelf processes and their interactions is critically important for a more comprehensive understanding of regional physical oceanography in the northern GoM. For this purpose, cross-scale models with unstructured grids become an attractive option.

70   The hydrodynamic conditions (e.g., salinity, stratification, and vertical mixing) over the Louisiana shelf is known to be dominated by the influence of the MAR plumes (Lehrter et al., 2013; Rong et al., 2014; Androulidakis et al., 2015). However, their effect on the salinity on the Texas shelf has not been well documented. Measurements at Port Aransas (600 km to the west of Atchafalaya River) show evident seasonal cycle, with higher salinity during the summer and lower salinity during the winter

75   (Bauer, 2002). Is this seasonality related to the seasonal variation of the MAR discharge and/or to the seasonality of the shelf transport? A broader question may be how the MAR discharge affects the salinity along the Texas coast. Furthermore, it is also important to understand the temporal and spatial scales with which the salinity at or near the mouth of an estuarine system respond to the river plumes from neighboring river systems. For example, how long will it take for the salinity at the Texas coast to

80   respond to a pulse of freshwater input from the MAR? This time scale in comparison to the time scales of estuarine processes (e.g., recovery time scale from storm disturbance) will allow one to determine whether the remote influence from neighboring major rivers is necessary to consider.

Here, we present a model for the northern GoM, with a domain including all the major estuaries as well as the shelf and a fine-resolution grid for local estuaries to resolve small-scale bathymetric or

85   geometric features such as ship channels and dikes. Using Galveston Bay as an example, we highlight the flexibility and capability of the model to simulate both estuarine and shelf dynamics. We demonstrate the importance of the interactions among estuaries and the shelf by investigating the remote influence of the MAR discharge on the hydrodynamics along the Texas coast.

2. Methodology

90 **2.1 Model description**

We employed the Semi-implicit Cross-scale Hydroscience Integrated System Model (SCHISM: Zhang et al., 2015, 2016), an open-source community-supported modeling system, derived from the early SELFE model (Zhang and Baptista, 2008). SCHISM uses highly efficient semi-implicit finite-element/finite-volume method with a Eulerian-Lagrangian algorithm to solve the turbulence-averaged

95 Navier-Stokes equations under the hydrostatic approximation. It uses the generic length-scale model of Umlauf and Burchard (2003) with the stability function of Kantha and Clayson (1994) for turbulence closure. One of the major advantages of the model is that it has the capability of employing a very flexible vertical grid system, robustly and faithfully resolving the complex topography in estuarine and oceanic systems without any smoothing (Zhang et al., 2016; Stanev et al., 2017; Du et al., 2018b; Ye et

100 al., 2018). A more detailed description of the SCHISM, including the governing equations, horizontal and vertical grids, numerical solution methods, and boundary conditions, can be found in Zhang et al. (2015, 2016).

2.2 Model domain and grid system

The model domain covers the Texas, Louisiana, Mississippi, and Alabama coasts, including the

105 shelf as well as major estuaries (e.g., Mobile Bay, Mississippi River, Atchafalaya River, Sabine Lake, Galveston Bay, Matagorda Bay, and Corpus Christi Bay) (Fig. 1). The domain also includes part of the deep ocean to set the open boundary far away from the shelf so as to avoid imposing boundary conditions at topographically complex locations. The horizontal grid contains 142,972 surface elements (triangular and quadrangular), with the resolution ranging from 10 km in the open ocean to 2.5 km on

110 average on the shelf (shallower than 200 m) to 40 m at the Houston Ship Channel, a narrow but deep channel along the longitudinal axis of Galveston Bay. The fine grid for the ship channel is carefully aligned with the channel orientation in order to accurately simulate the salt intrusion process (Ye et al., 2018). Vertically, a hybrid s-z grid is used, with 10 sigma layers for depths less than 20 m and another 30 z layers for depths from 20 to 4000 m (20, 25, 30, 35, 40, 50, 60, 70, 80, 90, 100, 125, 150, 200, 250,

115 300, 350, 400, 500, 600, 700, 800, 900, 1000, 1250, 1500, 2000, 2500, 3000, 4000 m); shaved cells are automatically added near the bottom in order to faithfully represent the bathymetry and thus the bottom-

controlled processes. This hybrid *s-z* vertical grid enables the model to better capture the stratification in the upper surface layer while keeping the computational cost reasonable for simulations of the deep waters. With a time step of 120 s and the TVD^2 scheme for mass transport, it takes about 24 hrs for one-year simulation with 120 processors (Intel Xeon E5-2640 v4).

The bathymetry used in the model is based on the coastal relief model (3 arc-second resolution: https://www.ngdc.noaa.gov). The local bathymetry in Galveston Bay is augmented by 10-m resolution DEM bathymetric data to resolve the narrow ship channel (150 m wide, 10-15 m deep) that extends from the bay entrance all the way to the Port of Houston. Bathymetry of the ship channels in other rivers, such as Mississippi, Atchafalaya, and Sabine rivers, is manually set following the NOAA navigational charts. The depth in the model domain ranges from 3400 m in the deep ocean to less than 1 m in Galveston Bay (Fig. 2).

2.3 Forcing conditions

The model was validated for the two-year conditions in 2007-2008 and was forced by the observed river discharge, reanalysis atmospheric forcing, and open boundary conditions from global HYCOM output. Daily freshwater inputs from the USGS gauging stations were specified at 15 river boundaries (Fig. 1). For the Mississippi River, the largest in the study area, river discharge at Baton Rouge, LA (USGS 07374000) was used. For the Atchafalaya River, the second largest, the discharge data at the upper river station (USGS 07381490 at Simmesport, LA) was used, but the data before 2009 at this station are not available. However, we found a significant linear relationship between this station and the one near the river mouth (USGS 07381600 at Morgan City, LA) with a 2-day time lag (r^2 of 0.92), based on the data from 2009 to 2017. The freshwater discharge estimated at Simmesport using this relationship for 2007-2008 was used to specify the Atchafalaya River freshwater input into the Atchafalaya Bay. For the Trinity River, the major river input for Galveston Bay, river discharge at the lower reach station at Wallisville (USGS 08067252) was used, where the mean river discharge (averaged over April 2014 and April 2018) is about 56% of that at an upper reach station at Romayor (USGS 08066500). This is because the water from Romayor likely flows into wetlands and water bodies surrounding the main channel of the Trinity River before reaching Wallisville (Lucena and Lee, 2017). The river discharge data at the Wallisville station are not available before April 2014. Similar to the case for Atchafalaya River, there is a significant linear relationship between these two stations (r^2 of 0.89 with a 4-day time lag based on the data from 2014 to 2018). The freshwater discharge for 2007-2008

estimated using this relationship was used to specify the Trinity River freshwater input into Galveston Bay. River flows from other rivers were prescribed using the data at the closest USGS stations. Water temperatures at the river boundaries were also based on the data at these USGS stations.

150   Reanalyzed 0.25° resolution, 6-hourly atmospheric forcing, including air temperature, solar radiation, wind, humidity, and pressure at mean sea level, were extracted from the European Centre for Medium-Range Weather Forecasts (ECMWF: https://www.ecmwf.int). SCHISM uses the bulk aerodynamic module of Zeng et al. (1998) to estimate heat flux at the air-sea interface. Both harmonic tide and subtidal water level were used to define the ocean boundary condition, with the harmonic tide
155   (M2, S2, K2, N2, O1, Q1, K1, and P1) from the global tidal model FES2014 (Carrere et al., 2015) and the subtidal water level from the low-pass filtered (cut-off period of 15 days) daily global HYCOM output. The model was relaxed during inflow to the HYCOM output at the ocean boundary in terms of salinity, temperature, and velocity.

2.4 Numerical experiments

160   To investigate the remote influence from the MAR discharge, we conducted three numerical experiments that use the same model configuration as in the realistic 2007-2008 model run except for freshwater discharge, wind forcing, initial salinity condition, and salinity boundary condition. To isolate the influence of the MAR discharge, we considered freshwater discharges (constant long-term means) only for Mississippi River, Atchafalaya River, and Galveston Bay, with no discharge from other coastal
165   systems. To examine the effect of seasonal wind, we chose the January 2008 and July 2008 winds as a representative of the winter and summer winds, respectively. The January wind was dominated by northeast-east wind and expected to induce a stronger downcoast (from Louisiana toward Texas) longshore current compared to the predominantly south wind in July (Fig. S1). The initial salinity condition is set to 36 psu throughout the entire domain and for all vertical layers. Salinity at the ocean
170   boundary is set to 36 psu throughout the simulation period.

Differences among the three experiments' settings are: (1) experiment *Jan-G* includes only the river discharges into Galveston Bay (259 m^3 s^{-1}) and uses the January 2008 wind; (2) experiment *Jan-GAM* includes both Galveston discharge as well as the MAR discharges (22,189 m^3 s^{-1}) and uses the January 2008 wind; and (3) experiment *Jul-GAM* has the same discharges as *Jan-GAM* but uses the July
175   2008 wind. In each simulation, the January or July wind was repeated every month, rather than using

monthly mean steady wind, in order to take into account the wind variability, which is known to play an important role on the shelf circulation (Ohlmann and Niiler, 2005).

3. Model validation

The model results of 2007-2008 were compared with observations for water level at seven
180   NOAA tidal gauge stations, salinity at four Texas Water Development Board (TWDB) stations, temperature at three NOAA stations, and current velocity at two Texas Automated Buoy System (TABS) buoys (see Fig. 2 for station locations). Comparisons were made for both total and subtidal (48-hr low-pass filtered) components. For quantitative assessment of the model performance, two indexes were used, model skill (Wilmott, 1981) and mean absolute error (*MAE*):

$$185 \quad Skill = 1 - \frac{\sum_{i=1}^{N} |X_{mod} - X_{obs}|^2}{\sum_{i=1}^{N} (|X_{mod} - \overline{X_{obs}}| + |X_{obs} - \overline{X_{obs}}|)^2} \tag{1}$$

$$MAE = \frac{1}{N} \sum_{i=1}^{N} |X_{mod} - X_{obs}| \tag{2}$$

where X_{obs} and X_{mod} are the observed and modeled values, respectively, with the overbar indicating the temporal average over the number of observations (*N*). *Skill* provides an index of model-observation agreement, with a skill of one indicating perfect agreement and a skill of zero indicating complete
190   disagreement. The magnitude of *MAE* indicates the average deviation between model and observation.

3.1 Water level

The model-observation comparisons were made for water level at stations along the coast and inside Galveston Bay. Manning's friction coefficient, which is converted to the bottom drag coefficient for the 3D simulation in the model, was used as a calibration parameter. The model results with a
195   spatially uniform Manning's coefficient of 0.016 $m^{1/3}$ s^{-1} shows a good agreement with the observational data. Overall, the model reproduces well both the tidal and subtidal components of water level at tidal gauge stations along the coast as well as inside Galveston Bay (Fig. 3, Table 1, and Fig. S2). The *MAE* is in the range of 7-8 cm and 5-7 cm for the total and subtidal components, respectively. The model skill varies spatially, with relatively low skills (0.88) at Pilot Station and Dauphin Island for the subtidal

component and high skills (≥ 0.94) at the stations in the Texas coast including Galveston Bay for both the total and subtidal components. It is interesting to note that the model has also simulated well the storm surge during Hurricane Ike (around day 625), one of the most severe hurricanes that hit the Houston-Galveston area in recent years. When applied to investigate the dramatic estuarine response to the Hurricane Harvey (2017) in Galveston Bay, this model successfully reproduced the long-lasting elevated water level inside the bay (Du et al., 2019a). Simulation of surface elevation is sensitive to topography, bottom friction, boundary conditions, and atmospheric forcings. Some discrepancies are expected due to the assumption of spatially uniform Manning's coefficient. Further improvement might be achieved by using spatially varying coefficients, but we did not deem it worth trying, considering the current satisfactory performance of the model. Additional discrepancies may come from the limited spatial and temporal resolution of atmospheric forcings, the accuracy of the bathymetric data, and the reliability of the open boundary conditions from the global HYCOM output.

3.2 Salinity

The model reproduces reasonably the observed variation in salinity at stations inside Galveston Bay (Fig. 4 and Table 1). The *MAEs* are no larger than 3 psu and the model skills range between 0.81-0.93 and 0.75-0.93 for the total and subtidal components, respectively. It is important to note that the salinity at the bay mouth under normal (i.e., non-flooding) condition is sensitive to the longshore transport of low salinity water from neighboring estuaries, such as nearby Sabine-Neches River, Atchafalaya River, and Mississippi River. Successful simulation of salinity at the bay mouth requires an accurate simulation of not only the bay-wide transport but also the longshore transport. Errors in the modeled salinity at the bay mouth can propagate to the upper bay. For example, salinity during days 60-100 is overestimated at the mouth (station BOLI) and this error propagated into the middle bay station (station MIDG) (Fig. 4). Discrepancies as large as 10 psu are not likely caused by inaccurate discharge from the Trinity River, as this river has a very limited influence on the salinity on the shelf (further discussed in Section 4.3). Unfortunately, with no data available for the vertical salinity profile, the model performance for the vertical mass transport cannot be evaluated. However, accurate simulation of the observed salinity at the mid-bay station provides alternative evidence supporting the model's validity in horizontal mass transport and salt intrusion.

The model also captures the sharp change in salinity during Hurricane Ike (around day 620). The salinity at the upper bay (Fig. 4b) decreased from 26 psu to 0 within two days, which was caused by a

230   pulse of freshwater discharge from Lake Houston (see reservoir storage at USGS 08072000). In

addition, the model reproduces well the spatial difference in the amplitude of tidal signal in salinity.

Salinity in Trinity Bay (Fig. 4a) shows very weak tidal signal while salinity at the bay mouth (Fig. 4d)

has much stronger tidal signal. Galveston Bay, in general, has micro-tidal ranges with a mean tidal range

of 0.3 m at the mid-bay station (Eagle Point in Fig. 2). The tidal signal, however, becomes stronger at

235   the narrow bay mouth (2.5 km wide), with the tidal current being as strong as 1 m s^{-1} (see station g06010

at http://pong.tamu.edu/tabswebsite/).

The modeled salinity was also compared to the observed salinity structure over the Texas-

Louisiana shelf using the data from the shelf-wide summer survey in July 2008 as an example (Fig. 5).

Both the horizontal and vertical structures of salinity on the shelf are well reproduced by the model, with

240   the *MAE* over 65 stations of 1 and 2 psu for the surface and bottom salinity, respectively. Data and

model consistently show relatively shallow halocline at section A (west of Mississippi Delta) and deeper

halocline at section F (off Atchafalaya Bay). The upper layer off Atchafalaya Bay was nearly well

mixed, which is also reproduced by the model, although the model somewhat underestimates the bottom

salinity at section F. In addition, the model also show there was little tidal variability of the vertical

245   salinity profile on the shelf (e.g., stations F4 and A7 in Fig. 5), which can be attributed to the small tidal

range in the northern GoM.

3.3 Temperature

The model reproduces well the observed temperatures at three NOAA stations located from the

Galveston Bay mouth to the upper bay (Fig. 6). Both the seasonal and diurnal cycles are well captured,

250   with the *MAEs* of about 1°C and model skills of 0.99. Even within a relatively small region inside

Galveston Bay, temperature can vary significantly. During days 300-350, for example, large fluctuations

in temperature occurred at the mid-bay station (Fig. 6b), while the fluctuations was smaller at the bay

entrance (Fig. 6a) or the upper bay (Fig. 6c). These spatiotemporal variations are reproduced well by the

model, demonstrating not only the good performance of the model but also the reliability of the

255   atmospheric forcing data.

The model performance in reproducing temperature over the Texas-Louisiana shelf was further

examined with the satellite data for sea surface temperature (SST). Seasonality of the SST extracted

from MODIS over the northern GoM is overall reproduced well (Fig. 7). It is worth noting that the

model also reproduces the relatively low temperatures on the southern Texas coast during summer,

260 which is a well-known upwelling zone during the summertime when upcoast (from Texas toward Louisiana) winds drive an offshore surface transport (Zavala-Hidalgo et al., 2003).

3.4 Shelf current

Shelf current plays a key role in transporting the low-salinity water originated from MAR, and it can be affected by not only the wind field but also the mesoscale eddies in the northern GoM. One of the
265 important features of the Texas-Louisiana shelf is the quasi-annual pattern of shelf current, which is predominantly westward for most of the time except during summer (Cochrane and Kelly, 1986; Li et al., 1997; Cho et al., 1998). The prominent downcoast shelf current is driven by along-shelf wind and enhanced by the MAR discharge (Oey, 1995; Li et al., 1997; Nowlin et al., 2005). Under summer wind that usually has an upcoast component, the nearshore current is reversed to the upcoast direction (Li et
270 al., 1997). Such seasonality also occurred during 2007-2008. The model reproduces well the observed subtidal component of surface longshore current at two TABS buoy stations outside of Galveston Bay, buoy B (~20 km offshore) and buoy F (~80 km offshore) (Fig. 8), with the *MAEs* of 8-14 cm s^{-1} and the model skills of 0.67-0.88 (Table 1).

4. Remote influence of the MAR discharge

275 The conditions in Texas coastal waters are impacted by several remote sources, including mesoscale eddies (Oey et al., 2005; Ohlmann and Niiler, 2005), longshore transport of low-salinity water from major rivers (Li et al., 1997; Nowlin et al., 2005), and Ekman transport induced by longshore wind and the resulting upwelling/downwelling (Li et al., 1997; Zhang et al., 2012). Here, based on the realistic model results and numerical experiments, we discuss the remote influence of major river
280 discharge and shelf dynamics on the longshore transport, salinity, stratification, and vertical mixing at the Texas coast, as well as the water exchange between the coastal ocean and local coastal system.

4.1 Variation in shelf current and salinity

The strength and direction of shelf current are sensitive to the wind field. Comparison of the model results on day 150 (May 31, 2007) and day 160 (June 10, 2007) clearly shows the different
285 distribution of lower-salinity water along the coast in response to wind field and the resulting shelf

current (Fig. 9). The river discharge differences between these two days are negligible and thus the differences in lower-salinity water distribution can be mainly attributed to the differences in shelf current. Day 150 was characterized by a significant downcoast shelf current in the inner shelf, with a current speed exceeding 0.5 m s^{-1}, while day 160 was characterized by a rather weak shelf current with a

290   speed of less than 0.1 m s^{-1}. The pattern of the surface residual current is related to the wind field. On day 150, a downcoast component of the wind induced an onshore Ekman transport, which in turn resulted in a downcoast geostrophic flow (Li et al., 1997). This downcoast flow transported the low-salinity water from MAR toward Texas while constraining it to a narrow band against the shoreline (Fig. 9e). Under weak or upcoast shelf current, in contrary, this constraining was weakened, leading to

295   offshore displacement of the low-salinity water (Fig. 9f). As a result, salinity on the Texas inner shelf was higher on day 160 than that on day 150.

        Regulated by the shelf current, salinity distribution over the shelf exhibits evident seasonality. The model results show that a narrow band of lower-salinity water persisted from Louisiana to the western Texas inner shelf during January-May 2008 (Fig. 10). The salinity at the Galveston Bay mouth

300   decreased by about 10 psu from January to May, which can be attributed to the increasing Mississippi discharge from January to May in 2008 (Mississippi discharge data at https://waterdata.usgs.gov/usa/nwis/uv?site_no=07374000). Starting from June 2008, the salinity along western Texas shelf gradually increased as the higher-salinity water from the southwestern boundary moved upcoast. The salinity at the Galveston Bay mouth increased from less than 20 psu in June to >30

305   psu in August (Fig. 10), about the same magnitude of salinity change from January to May. It suggests that the influence on the salinity in the Texas coast from the seasonally varying shelf circulation is comparable to that from the seasonal variation in the MAR discharge.

4.2 Influence of the MAR discharge on shelf transport and salinity

        The longshore transport plays a key role in redistributing the freshwater from the estuarine bays

310   along the shelf. The results from three numerical experiments show that, under the January wind, the downcoast longshore transport at four selected cross-shelf sections varies little among each other. The longshore transport is enhanced by the MAR discharge (long-term mean) by 10-14% (~80,000 m^3 s^{-1}), about four times the long-term mean river discharges from MAR (~22,000 m^3/s) (Fig. 11). The transport, however, is greatly reduced under the July wind and it decreases downcoast, with the

315   magnitude being one order smaller on the Texas shelf compared to that under the January wind. The

difference in longshore transport is related to the shelf circulations, which exhibit distinctly different patterns under different wind conditions (Fig. S3). Under the January wind, the surface shelf current flows downcoast, while under the July wind, it is weak and mainly in a direction normal to the coastline, resulting in a much smaller longshore transport.

320   The influence of the MAR discharge on the shelf salinity also depends on the wind condition and the resulting shelf current. Surface salinity maps averaged over days 250-300 show distinctly different spatial patterns of the lower-salinity water under different wind conditions (Fig. 12). The patterns are similar to the results from the 2007-2008 realistic run (Fig. 10). Under the winter wind, the lower-salinity water is trapped nearshore by the shelf current, forming a narrow band along the coast. Under

325   the summer wind, on the other hand, water on the Texas shelf is replenished by the saltier water originated from the southwest, leading to a tongue-shaped saltier-water intrusion toward the lower salinity water over Louisiana shelf. Consequently, salinity is higher on the Texas shelf and lower on the Louisiana shelf when compared to that under the winter wind.

4.3 Influence of the MAR discharge on Texas coast: salinity, stratification, and mixing

330   Numerical experiments reveal different time and spatial scales with which the surface salinity in Texas coastal water responds to the MARS discharge (Fig. 13). At the Galveston Bay mouth, the salinity begins to decrease from about day 25 in response to the MAR discharge and continues to decrease until around day 100 when it reaches a quasi-steady state. The MAR discharge (long-term mean) reduces the salinity by about 10 psu under the January wind but only by 5-6 psu under the July wind. Further south

335   at the Port Aransas mouth, the response time doubles to about 50 days, with the MAR discharge reducing the salinity by about 6 psu under the January wind. Salinity changes little in response to the discharges from Galveston Bay or the MAR discharge under July wind. As the influence from Galveston Bay is very limited at the Aransas Bay mouth even under a downcoast wind, it is reasonable to assume the influence will be even smaller under an upcoast wind.

340   Vertical profiles of salinity along a section from the Trinity Bay, along the Houston Ship Channel and the adjoining shelf show that the MAR discharge increases salinity stratification on the shelf (Fig. 14). The lower-salinity water along the coastline increases the cross-shelf baroclinic pressure gradient, leading to a stronger stratification. The distinctive difference exists between *Jan-GAM* and *Jul-GAM*. A stronger stratification on the inner shelf appears under the July wind, with the bottom-surface

345   salinity difference as large as 4 psu. Vertical mixing on the inner Texas shelf is weakened due to the

MAR discharge, particularly under July wind. The vertical diffusivities are one or two orders smaller in

magnitude than those under the January wind. Under the July wind, the stratification along the ship

channel becomes stronger, probably because of a larger salinity near the bay mouth and/or a weaker

wind in July with a mean speed of 4.79 m s^{-1} relative to a mean speed of 6.88 m s^{-1} in January (Fig. S1).

350   A larger salinity near the mouth induces a stronger horizontal salinity gradient, leading to a stronger

circulation and stratification.

4.4 Influence of the MAR discharge on estuarine-coastal exchange

Salinity change due to the remote river input and shift in wind field affects the estuarine

dynamics, such as estuarine circulation, salt flux, and estuarine-coastal exchange. We examined the

355   change in exchange flow and salinity at the Galveston Bay mouth due to remote river influence and

different shelf current. Following Lerzak et al. (2006), we calculated the tidally averaged and cross-

sectionally varying components (u_e and S_e) from the along-channel velocity u and salinity S. From the

vertical profiles of u_e and S_e at the deepest part between the two jetties at the bay mouth, it is evident that

in the lower layer u_e is strongest (maximum of 6 cm s^{-1}) and S_e is largest (maximum of 0.95 psu) for the

360   case *Jan-G*, indicating the strongest exchange flow (i.e., estuarine circulation), compared to the other

two cases with the MAR discharge (Fig. 15). On the contrary, the case *Jan-GAM* shows the weakest

bottom u_e (maximum of 4 cm s^{-1}) and the smallest bottom S_e (maximum of 0.60 psu). The MAR

discharge under the January wind condition decreases the salinity at the bay mouth the most and results

in the weakest horizontal salinity gradient and exchange flow.

365   The influence of the MAR discharge on the dynamics of Galveston Bay was further examined

using total exchange flow (TEF). Using the isohaline framework method proposed by MacCready

(2011), which was found to be a precise way to quantify the landward salt transport (Chen et al., 2012).

In this method, the tidally averaged volume flux of water with salinity greater than s is defined as:

$$Q(s) = \left\langle \int_{A_s} u \, dA \right\rangle \tag{3}$$

370   where A_s is the tidally varying portion of the cross-section with salinity larger than s. In our case, we

calculated $Q(s)$ for the salinity bins from 0 to 35 psu with an interval of 0.5 psu. The volume flux in a

specific salinity class is defined as:

$$-\frac{\partial Q}{\partial s} = -\lim_{\delta s \to 0} \frac{Q(s + \delta s / 2) - Q(s - \delta s / 2)}{\delta s} \tag{4}$$

where the minus sign indicates that a positive value of $-\partial Q / \partial s$ corresponds to inflow for a given salinity class. The total exchange flow (Q_{in}), the flux of water into the estuary due to all tidal and subtidal processes, is then calculated as:

$$Q_{in} \equiv \int \frac{-\partial Q}{\partial s}\Big|_{in} ds \tag{5}$$

The resulting salt flux into the estuary (F_{in}) is given by:

$$F_{in} = \int s(-\frac{\partial Q}{\partial s})\Big|_{in} ds \tag{6}$$

and the ratio of salt mass inside the estuary to the salt influx gives the mean residence time (T_{res}):

$$T_{res} = \frac{\int s dV}{F_{in}} \tag{7}$$

where V is the estuarine volume.

Table 2 lists the values of Q_{in}, F_{in}, and T_{res} for three numerical experiments. For the exchange flow, Q_{in} is largest for the case *Jan-G* and smallest for the case *Jan-GAM*. The MAR discharge under the January wind condition causes the largest decrease in salinity at the Galveston Bay mouth (Fig. 13a), effectively slowing down the water exchange between the bay and coastal ocean. The reduction in Q_{in} caused by the remote discharge (470 m^3 s^{-1} = 24% reduction) is 1.8 times the long-term mean river input into Galveston Bay (259 m^3 s^{-1}). Moreover, F_{in} for the case *Jan-GAM* is about half of that in the case *Jan-G*. As a result, T_{res} of the bay is largest in the case *Jan-GAM*, although the difference in T_{res} is not as large as that in F_{in} because the bay has the smallest salt mass in the case *Jan-GAM* (Table 2). This analysis also suggests that the exchange between the bay and coastal ocean is likely stronger during summer than during winter under the same river discharge condition.

5. Summary

An unstructured-grid hydrodynamic model with a hybrid vertical grid was developed and validated for water level, current velocity, salinity, and temperature for Galveston Bay as well as over the shelf in northern GoM. The good model performance, particularly in terms of salinity (vertically/horizontally), is at least in part attributable to the inclusion of multiple river plumes along the

coastline as well as the interaction between estuaries and shelf. This model provides a good platform that can be used for other purposes in future studies. Its flexibility in the horizontal and vertical grids allows refinement in any region of interest without penalty in the time step (due to the semi-implicit scheme). For example, it would be relatively easy to adapt the model by refining the grid inside any target bay, e.g., Corpus Christi Bay.

The 2007-2008 model run reveals the seasonally varying influence of the MAR discharge on the Texas shelf. Three numerical experiments were carried out to examine the extent to which the major rivers in the region influence local coastal bay systems in Texas. The MAR discharge has great influence on the salinity regime along the Texas coast and its influence depends on the wind-controlled shelf circulation. Winter wind drives a stronger downcoast longshore transport with its magnitude at least one order larger than that under summer wind. The MAR discharge (long-term mean) enhances the downcoast transport by 10-14% under winter wind, lowers the salinity by up to 10 psu at the mouth of Galveston Bay and 6 psu at the mouth of Port Aransas. Vertical mixing is also sensitive to wind forcing. Summer wind tends to displace the low-salinity water further offshore, while the winter wind constrains the low-salinity water to a narrow band against the shoreline. As a result, the stratification is stronger and vertical mixing is weaker over the shelf during summer. Lower salinity condition on the Texas shelf decreases the longitudinal salinity gradient at the bay mouth, leading to a weakened estuarine circulation and weaker salt exchange.

This study demonstrates the necessity of including the remote influence from the MAR discharge for the modeling of the Texas coastal systems, particularly for processes associated with relatively long time scales (e.g., months). Receiving relatively small freshwater discharge and limited by narrow outlets and small tidal ranges, the estuarine bay systems along the Texas coast, e.g., Galveston Bay, Aransas Bay, and Corpse Christi Bay, are characterized by relatively slow water exchange and long flushing times. In this study, we show that the exchange flow plays an important role for the water renewal and that the exchange flow varies greatly depending on the wind field and the resulting shelf current. Modulation by the MAR discharge, when coupled with downcoast wind conditions, could have a great influence on the dynamics of estuaries along the Texas coast.

425 **Author contributions**

J. Du and K. Park led the effort of model development, data analysis, and preparation of the manuscript. J. Shen, Y. J. Zhang, F. Ye, and Z. Wang provided guidelines for the model configuration in terms of preparation of forcing files and boundary conditions. X. Yu assisted the visualization of modeled and observed data. N. N. Rabalais provided the shelf-wide survey data for the model
430 validation. All authors were involved in the manuscript writing.

Acknowledgements:

All the observational data used for model validation are available online. Salinity data are extracted from TDWB (https://waterdatafortexas.org/coastal). Contiguous monitoring data of temperature and water level are extracted from NOAA Tide and Current
435 (https://tidesandcurrents.noaa.gov/). Surface buoy current data are extracted from TABS (http://pong.tamu.edu/tabswebsite/). Daily satellite data (4 km resolution) are extracted from (https://podaac.jpl.nasa.gov/). Shelf-wide summer survey data of 2008 is accessible at NODC with the accession number of 0069471 (https://www.data.gov/). The numerical simulation was performed on the high-performance computer cluster at the College of William and Mary.

440 **Reference:**

Androulidakis Y. S., Kourafalou V. H., and Schiller R. V.: Process studies on the evolution of the Mississippi River plume: Impact of topography, wind and discharge conditions, Cont. Shelf Res., 107, 33-49, https://doi.org/10.1016/j.csr.2015.07.014, 2015

Barkan, R., McWilliams, J. C., Shchepetkin, A. F., Molemaker, M. J., Renault, L., Bracco, A., and Choi,
445 J.: Submesoscale dynamics in the northern Gulf of Mexico. Part I: Regional and seasonal characterization, and the role of river outflow, J. Phys. Oceanogr., 47, 2325-2346, https://doi.org/10.1175/JPO-D-17-0035.1, 2017

Bauer, R. T.: Reproductive ecology of a protandric simultaneous hermaphrodite, the Shrimp Lysmata Wurdemanni (Decapoda: Caridea: Hippolytidae), J. Crustac. Biol., 22, 742-749,
450 https://doi.org/10.1163/20021975-99990288, 2002

Bianchi, T. S., DiMarco, S. F., Cowan, J. H., Hetland, R. D., Chapman, P., Day, J. W., and Allison, M. A.: The science of hypoxia in the northern Gulf of Mexico: A review, Sci. Total Environ., 408(7), 1471–1484, https://doi.org/10.1016/j.scitotenv.2009.11.047, 2010

Bracco, A., Choi, J., Joshi, K., Luo, H., and McWilliams, J. C.: Submesoscale currents in the northern
455   Gulf of Mexico: Deep phenomena and dispersion over the continental slope, Ocean Model., 101,
43–58, https://doi.org/10.1016/j.ocemod.2016.03.002, 2016

Carrere, L., Lyard, F., Cancet, M., and Guillot, A.: FES 2014, a new tidal model on the global ocean
with enhanced accuracy in shallow seas and in the Arctic region, In: Abstracts of the EGU General
Assembly 2015, Vienna, Austria, April 12-17, 2015,
460   http://adsabs.harvard.edu/abs/2015EGUGA..17.5481C, 2015

Chen, C., Beardsley, R. C., and Cowles, G.: An unstructured grid, finite-volume coastal ocean model
(FVCOM) system, Oceanography, 19(1), 78–89, https://doi.org/10.5670/oceanog.2006.92, 2006

Chen, S.-N., Geyer, W. R., Ralston, D. K., and Lerczak, J. A.: Estuarine exchange flow quantified with
isohaline coordinates: Contrasting long and short estuaries, J. Phys. Oceanogr., 42(5), 748–763,
465   https://doi.org/10.1175/JPO-D-11-086.1, 2012

Cho, K., Reid, R. O., and Nowlin, Jr., W. D.: Objectively mapped stream function fields on the Texas-
Louisiana shelf based on 32 months of moored current meter data, J. Geophy. Res., 103(C5),
10377-10390, https://doi.org/10.1029/98JC00099, 1998

Chu, P. P., Ivanov, L. M., and Melnichenko, O. V.: Fall-winter current reversals on the Texas-Louisiana
470   continental shelf, J. Phys. Oceanogr., 35(5), 902–910, https://doi.org/10.1175/JPO2703.1, 2005

Cochrane, J. D., and Kelly, F. J.: Low-frequency circulation on the Texas-Louisiana continental shelf, J.
Geophy. Res., 91(C9), 10645-10659, https://doi.org/10.1029/JC091iC09p10645, 1986

DiMarco, S. F., Howard, M. K., and Reid, R. O.: Seasonal variation of wind-driven diurnal current
cycling on the Texas-Louisiana continental shelf, Geophy. Res. Lett., 27(7), 1017–1020,
475   https://doi.org/10.1029/1999GL010491, 2000

Du, J., Park, K., Shen, J., Dzwonkowski, B., Yu, X., and Yoon, B. I. (2018a). Role of baroclinic
processes on flushing characteristics in a highly stratified estuarine system, Mobile Bay, Alabama,
J. Geophy. Res.: Oceans, 123, 4518-4537, https://doi.org/10.1029/2018JC013855, 2018a

Du, J., Shen, J., Zhang, Y. J., Ye, F., Liu, Z., Wang, Z., Wang, Y. P., Yu, X., Sisson, M., and Wang, H.
480   V. (2018b). Tidal response to sea-level rise in different types of estuaries: The importance of length,
bathymetry, and geometry, Geophy. Res. Lett., 45, 227-235,
https://doi.org/10.1002/2017GL075963, 2018b

Du, J., Park, K.: Estuarine salinity recovery from an extreme precipitation event: Hurricane Harvey in
Galveston Bay, Sci. Total Environ., 670, 1049-1059,
485   https://doi.org/10.1016/j.scitotenv.2019.03.265, 2019a

Du, J., Park, K., Dellapenna, T. M., and Clay, and J. M.: Dramatic hydrodynamic and sedimentary
responses in Galveston Bay and adjacent inner shelf to Hurricane Harvey, Sci. Total Environ., 653,
554-564, https://doi.org/10.1016/j.scitotenv.2018.10.403, 2019b

Dukhovskoy, D. S., Morey, S. L., Martin, P. J., O'Brien, J. J., and Cooper, C.: Application of a
490   vanishing, quasi-sigma, vertical coordinate for simulation of high-speed, deep currents over the
Sigsbee Escarpment in the Gulf of Mexico, Ocean Model., 28, 250-265,
https://doi.org/10.1016/j.ocemod.2009.02.009, 2009

Dzwonkowski, B., Park, K., and Collini, R.: The coupled estuarine-shelf response of a river-dominated system during the transition from low to high discharge, J. Geophy. Res.: Oceans, 120, 6145-6163, https://doi.org/10.1002/2015JC010714, 2015

Fennel, K., Hetland, R., Feng, Y., and Dimarco, S.: A coupled physical-biological model of the Northern Gulf of Mexico shelf: Model description, validation and analysis of phytoplankton variability, Biogeosciences, 8(7), 1881–1899, https://doi.org/10.5194/bg-8-1881-2011, 2011

Gierach, M. M., Vazquez-Cuervo, J., Lee, T., and Tsontos, V. M.: Aquarius and SMOS detect effects of an extreme Mississippi River flooding event in the Gulf of Mexico. Geophy, Res. Lett., 40(19), 5188–5193, https://doi.org/10.1002/grl.50995, 2013

Hetland, R. D., and DiMarco, S. F.: How does the character of oxygen demand control the structure of hypoxia on the Texas-Louisiana continental shelf? J. Mar. Sys., 70(1–2), 49–62, https://doi.org/10.1016/j.jmarsys.2007.03.002, 2008

Huang, W. J., Cai, W.-J., Castelao, R. M., Wang, Y., and Lohrenz, S. E.: Effects of a wind-driven cross-shelf large river plume on biological production and CO_2 uptake on the Gulf of Mexico during spring, Limnol. Oceanogr., 58(5), 1727–1735, https://doi.org/10.4319/lo.2013.58.5.1727, 2013

Justić, D., Rabalais, N. N., and Turner, R. E.: Effects of climate change on hypoxia in coastal waters: A doubled CO_2 scenario for the northern Gulf of Mexico, Limnol. Oceanogr., 41(5), 992–1003, https://doi.org/10.4319/lo.1996.41.5.0992, 1996

Kantha, L. H., and Clayson, C. A.: An improved mixed layer model for geophysical applications, J. Geophy. Res., 99(C12), 25235-25266, https://doi.org/10.1029/94JC02257, 1994

Kim, C.-K., and Park, K.: A modeling study of water and salt exchange for a micro-tidal, stratified northern Gulf of Mexico estuary, J. Mar. Sys., 96–97, 103–115, https://doi.org/10.1016/j.jmarsys.2012.02.008, 2012

Kuitenbrouwer, D., Reniers, A., MacMahan, J., and Roth, M. K.: Coastal protection by a small scale river plume against oil spills in the Northern Gulf of Mexico, Cont. Shelf Res., 163, 1–11, https://doi.org/10.1016/j.csr.2018.05.002, 2018

Laurent, A., Fennel, K., Hu, J., and Hetland, R.: Simulating the effects of phosphorus limitation in the Mississippi and Atchafalaya river plumes, Biogeosciences, 9(11), 4707–4723, https://doi.org/10.5194/bg-9-4707-2012, 2012

Lehrter, J. C., Ko, D. S., Murrell, M. C., Hagy, J. D., Schaeffer, B. A., Greene, R. M., Gould, R. W., and Penta, B.: Nutrient distributions, transports, and budgets on the inner margin of a river-dominated continental shelf, J. Geophy. Res.: Oceans, 118, 4822–4838, https://doi.org/10.1002/jgrc.20362, 2013

Lerczak, J., Geyer, W. R., and Chant, R. J.: Mechanisms driving the time-dependent salt flux in a partially stratified estuary, J. Phys. Oceanogr., 36, 2296–2311, https://doi.org/10.1175/JPO2959.1, 2006

Li, Y., Nowlin, Jr., W. D., and Reid, R. O.: Mean hydrographic fields and their interannual variability over the Texas-Louisiana continental shelf in spring, summer, and fall, J. Geophy. Res., 102(C1), 1027–1049, https://doi.org/10.1029/96JC03210, 1997

Lucena, Z., and Lee, M. T.: Characterization of Streamflow, Suspended Sediment, and Nutrients Entering Galveston Bay from the Trinity River, Texas, May 2014–December 2015, U.S. Geological Survey Scientific Investigations Report 2016–5177, 38, https://doi.org/10.3133/sir20165177, 2017

535 MacCready, P.: Calculating estuarine exchange flow using isohaline coordinates, J. Phys. Oceanogr., 41(6), 1116–1124, https://doi.org/10.1175/2011JPO4517.1, 2011

Martin, P. J.: Description of the Navy Coastal Ocean Model Version 1.0, NRL Report NRL/FR/7322–00–9962, Naval Research Laboratory, Stennis Space Center, MS, 2000

Nowlin, Jr., W. D., Jochens, A. E., Dimarco, S. F., Reid, R. O., and Howard, M. K.: Low-frequency
540 circulation over the Texas-Louisiana continental shelf, in: Circulation in the Gulf of Mexico: Observations and Models, edited by Sturges, W. and Lugo-Fernandez, A., Geophysical Monograph Series 161, AGU, Washington, DC, 219–240, https://doi.org/10.1029/161GM17, 2005

Oey, L.-Y.: Eddy- and wind-forced shelf circulation, J. Geophy. Res., 100(C5), 8621–8637, https://doi.org/10.1029/95JC00785, 1995

545 Oey, L.-Y., and Lee, H.-C.: Deep eddy energy and topographic Rossby waves in the Gulf of Mexico, J. Phys. Oceanogr., 32(12), 3499–3527, https://doi.org/10.1175/1520-0485(2002)032<3499:DEEATR>2.0.CO;2, 2002

Oey, L.-Y., Ezer, T., and Lee, H.-C.: Loop current, rings and related circulation in the Gulf of Mexico: A review of numerical models and future challenges, in: Circulation in the Gulf of Mexico:
550 Observations and Models, edited by Sturges, W. and Lugo-Fernandez, A., Geophysical Monograph Series 161, AGU, Washington, DC, 31–56, https://doi.org/10.1029/161GM04, 2005

Ohlmann, J. C., and Niiler, P. P.: Circulation over the continental shelf in the northern Gulf of Mexico, Prog. Oceanogr., 64(1), 45–81, https://doi.org/10.1016/j.pocean.2005.02.001, 2005

Rabalais, N. N., Turner, R. E., Justić, D., Dortch, Q., Wiseman, W. J., and Sen Gupta, B. K.: Nutrient
555 changes in the Mississippi River and system responses on the adjacent continental shelf, Estuaries, 19(2B), 386-407, https://doi.org/10.2307/1352458, 1996

Rabalais, N. N., Turner, R. E., and Scavia, D.: Beyond science into policy: Gulf of Mexico hypoxia and the Mississippi River, BioScience, 52(2), 129–142, https://doi.org/10.1641/0006-3568(2002)052[0129:BSIPGO]2.0.CO;2, 2002

560 Rabalais, N. N., Turner, R. E., Sen Gupta, B. K., Boesch, D. F., Chapman, P., and Murrell, M. C.: Hypoxia in the northern Gulf of Mexico: Does the science support the plan to reduce, mitigate, and control hypoxia? Estuaries Coast., 30(5), 753–772, https://doi.org/10.1007/BF02841332, 2007

Rayson, M. D., Gross, E. S., and Fringer, O. B.: Modeling the tidal and sub-tidal hydrodynamics in a shallow, micro-tidal estuary, Ocean Model., 89, 29–44,
565 https://doi.org/10.1016/j.ocemod.2015.02.002, 2015

Rego, J. L., and Li, C.: Storm surge propagation in Galveston Bay during Hurricane Ike, J. Mar. Sys., 82(4), 265–279, https://doi.org/10.1016/j.jmarsys.2010.06.001, 2010

Rong, Z., Hetland, R. D., Zhang, W., and Zhang, X.: Current-wave interaction in the Mississippi-Atchafalaya river plume on the Texas-Louisiana shelf, Ocean Model., 84, 67–83,
570 https://doi.org/10.1016/j.ocemod.2014.09.008, 2014

Sebastian, A., Proft, J., Dietrich, J. C., Du, W., Bedient, P. B., and Dawson, C. N.: Characterizing hurricane storm surge behavior in Galveston Bay using the SWAN+ADCIRC model, Coast. Eng., 88, 171–181, https://doi.org/10.1016/j.coastaleng.2014.03.002, 2014

Shchepetkin, A. F., and McWilliams, J. C.: The regional oceanic modeling system (ROMS): A split-explicit, free-surface, topography-following-coordinate oceanic model, Ocean Model., 9(4), 347–404, https://doi.org/10.1016/j.ocemod.2004.08.002, 2005

Stanev, E. V., Grashorn, S., and Zhang, Y. J.: Cascading ocean basins: Numerical simulations of the circulation and interbasin exchange in the Azov-Black-Marmara-Mediterranean Seas system, Ocean Dyn., 67(8), 1003-1025, https://doi.org/10.1007/s10236-017-1071-2, 2017

Umlauf, L., and Burchard, H.: A generic length-scale equation for geophysical turbulence models, J. Mar. Res., 61(2), 235–265, https://doi.org/10.1357/002224003322005087, 2003

Wang, D.-P., Oey, L.-Y., Ezer, T., and Hamilton, P.: Near-surface currents in DeSoto Canyon (1997–99): Comparison of current meters, satellite observation, and model simulation, J. Phys. Oceanogr., 33(1), 313–326, https://doi.org/10.1175/1520-0485(2003)033<0313:NSCIDC>2.0.CO;2, 2003

Wang, L., and Justić, D.: A modeling study of the physical processes affecting the development of seasonal hypoxia over the inner Louisiana-Texas shelf: Circulation and stratification, Cont. Shelf Res., 29, 1464-1476, https://doi.org/10.1016/j.csr.2009.03.014, 2009

Warrick, J. A. and Farnsworth, K. L.: Coastal river plumes: Collisions and coalescence, Prog. Oceanogr., 151, 245-260, https://doi.org/10.1016/j.pocean.2016.11.008, 2017

Willmott, C. J.: On the validation of models, Phys. Geogr., 2(2), 184–194, https://doi.org/10.1080/02723646.1981.10642213, 1981

Ye, F., Zhang, Y. J., Wang, H. V., Friedrichs, M. A. M., Irby, I. D., Alteljevich, E., Valle-Levinson, A., Wang, Z., Huang, H., Shen, J. and Du, J.: A 3D unstructured-grid model for Chesapeake Bay: Importance of bathymetry, Ocean Model., 127, 16–39, https://doi.org/10.1016/j.ocemod.2018.05.002, 2018

Zavala-Hidalgo, J., Morey, S. L., and O'Brien, J. J.: Seasonal circulation on the western shelf of the Gulf of Mexico using a high-resolution numerical model, J. Geophy. Res., 108(C12), 3389, https://doi.org/10.1029/2003JC001879, 2003

Zavala-Hidalgo, J., Gallegos-García, A., Martínez-López, B., Morey, S. L., and O'Brien, J. J.: Seasonal upwelling on the western and southern shelves of the Gulf of Mexico, Ocean Dyn., 56(3–4), 333–338, https://doi.org/10.1007/s10236-006-0072-3, 2006

Zhang, X., Hetland, R. D., Marta-Almeida, M., and DiMarco, S. F.: A numerical investigation of the Mississippi and Atchafalaya freshwater transport, filling and flushing times on the Texas-Louisiana shelf, J. Geophy. Res., 117, C11009, https://doi.org/10.1029/2012JC008108, 2012

Zhang, Y., and Baptista, A. M.: SELFE: A semi-implicit Eulerian-Lagrangian finite-element model for cross-scale ocean circulation, Ocean Model., 21(3–4), 71–96, https://doi.org/10.1016/j.ocemod.2007.11.005, 2008

Zhang, Y. J., Ateljevich, E., Yu, H. C., Wu, C. H., and Yu, J. C. S.: A new vertical coordinate system for a 3D unstructured-grid model, Ocean Model., 85, 16–31, https://doi.org/10.1016/j.ocemod.2014.10.003, 2015

Zhang, Y. J., Ye, F., Stanev, E. V, and Grashorn, S.: Seamless cross-scale modeling with SCHISM, Ocean Model., 102, 64–81, https://doi.org/10.1016/j.ocemod.2016.05.002, 2016

Zeng, X., Zhao, M., and Dickinson, R. E.: Intercomparison of bulk aerodynamic algorithms for the computation of sea surface fluxes using TOGA COARE and TAO data, J. Clim., 11, 2628-2644, https://doi.org/10.1175/1520-0442(1998)011<2628:IOBAAF>2.0.CO;2, 1998

615

Table 1: Error estimates for model-data comparison for 2007-2008.

Variables	Station	Total		Subtidal	
		MAE	Skill	MAE	Skill
Water level (cm)	Morgan's Point	7.61	0.96	6.65	0.95
	Eagle's Point	6.87	0.96	6.13	0.96
	Bay Entrance	7.98	0.96	6.17	0.94
	Freeport	7.62	0.96	6.37	0.94
	Bob Hall	6.65	0.97	5.41	0.94
	Pilot Station	6.23	0.95	5.36	0.88
	Dauphin Island	7.29	0.94	6.61	0.88
Salinity (psu)	TRIN (1.5 m)[a]	2.06	0.93	2.03	0.93
	BAYT (2.0 m)[a]	2.69	0.87	2.59	0.87
	MIDG (3.1 m)[a]	2.56	0.86	2.43	0.85
	BOLI (2.9 m)[a]	3.04	0.81	2.92	0.75
Surface temperature (°C)	Morgan's Point	0.93	0.99	0.92	0.99
	Eagle's Point	1.27	0.99	1.26	0.99
	Bay Entrance	0.91	0.99	0.86	0.99
Surface velocity (m s^{-1})	Buoy B	0.14	0.88	0.11	0.82
	Buoy F	0.10	0.79	0.08	0.67

[a] The value within the parenthesis indicates the mean depth below surface of the sensor.

620

Table 2: Total exchange flow (Q_{in}) and the resulting salt flux (F_{in}) at the Galveston Bay mouth, and the mean residence time of the bay (T_{res}) based on the isohaline method in MacCready (2011).

Case ID[a]	Q_{in} (m³ s⁻¹)	F_{in} (kg salt s⁻¹)	T_{res} (days)	S_{mean}[b] (psu)
Jan-G	1.93×10^3	6.75×10^4	13.0	20
Jan-GAM	1.46×10^3	3.47×10^4	16.0	13
Jul-GAM	1.80×10^3	5.30×10^4	13.1	16

625 [a] see Fig. 11 for the explanation of idealized runs
[b] Mean salinity (volume-weighted average over days 250-300) inside the bay
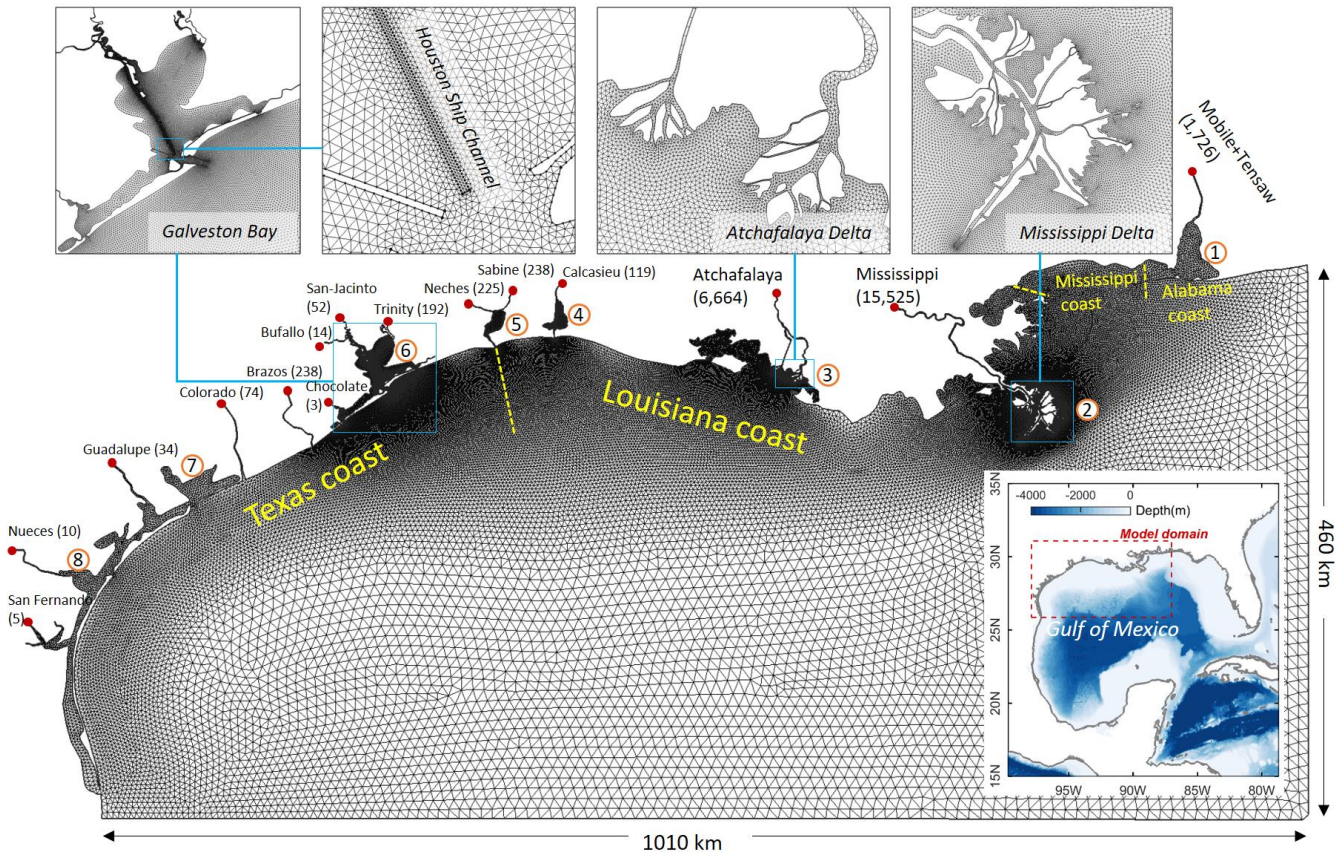
Figure 1: The model domain and the horizontal grid, with the upper panels showing zoom-ins of selected coastal systems. Locations of major river inputs are indicated with red dots, with the associated mean river discharges ($m^3 s^{-1}$) shown in the parentheses. Major estuarine bay systems in the model domain include Mobile Bay (1), Mississippi River (2), Atchafalaya River (3), Calcasieu Lake (4), Sabine Lake (5), Galveston Bay (6), Matagorda Bay (7), and Corpus Christi Bay (8).
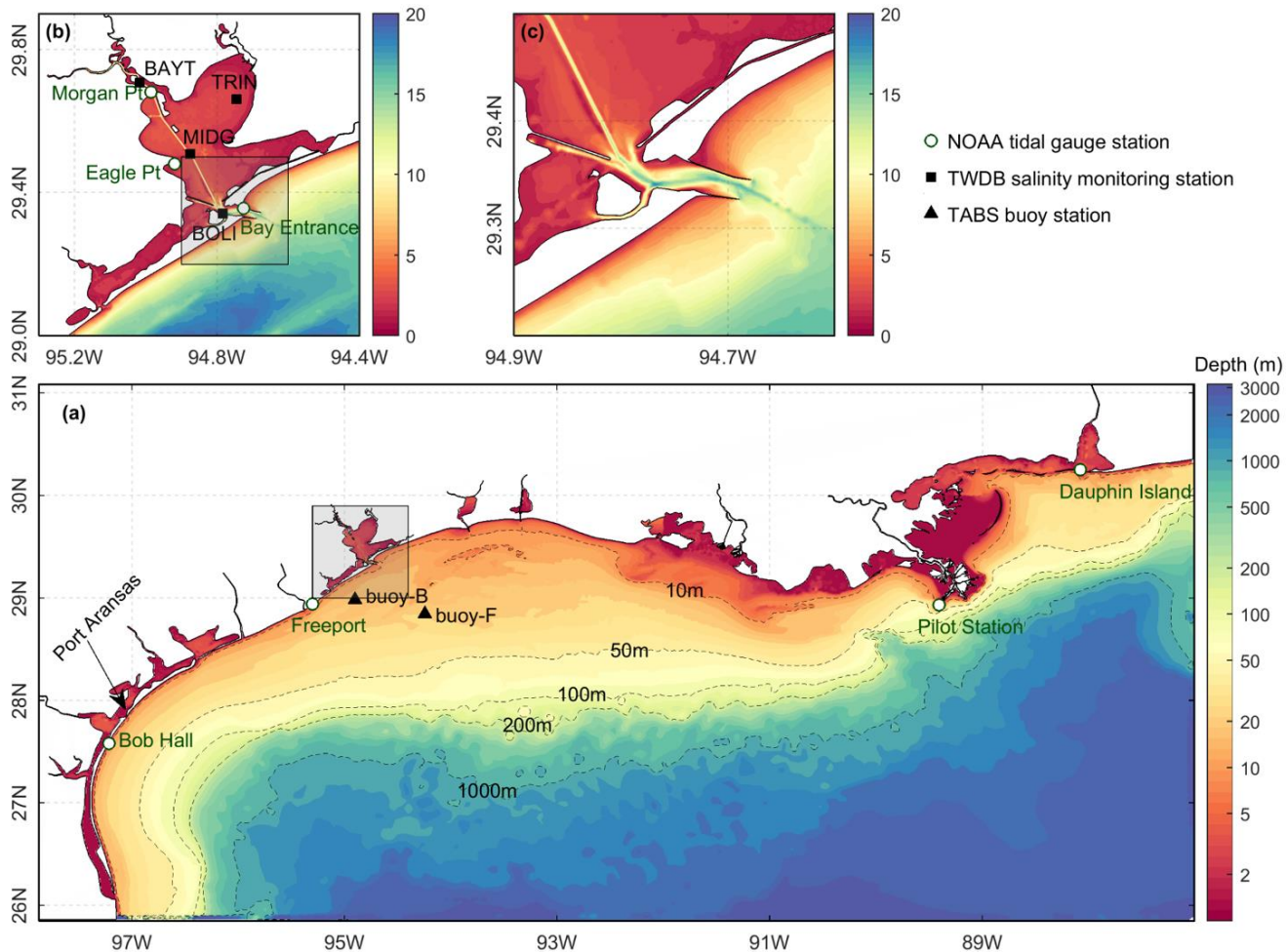
Figure 2: Bathymetry in the model domain with the upper panels showing zoom-ins of Galveston Bay and its main entrance. Note that the lower panel uses the log scale for depth because of a very wide range of depth over the entire model domain. Also shown are the NOAA tidal gauge stations (open green circles), TWDB (Texas Water Development Board) salinity monitoring stations (solid black circles), and TABS (Texas Automated Buoy System) buoy stations (black solid triangles).
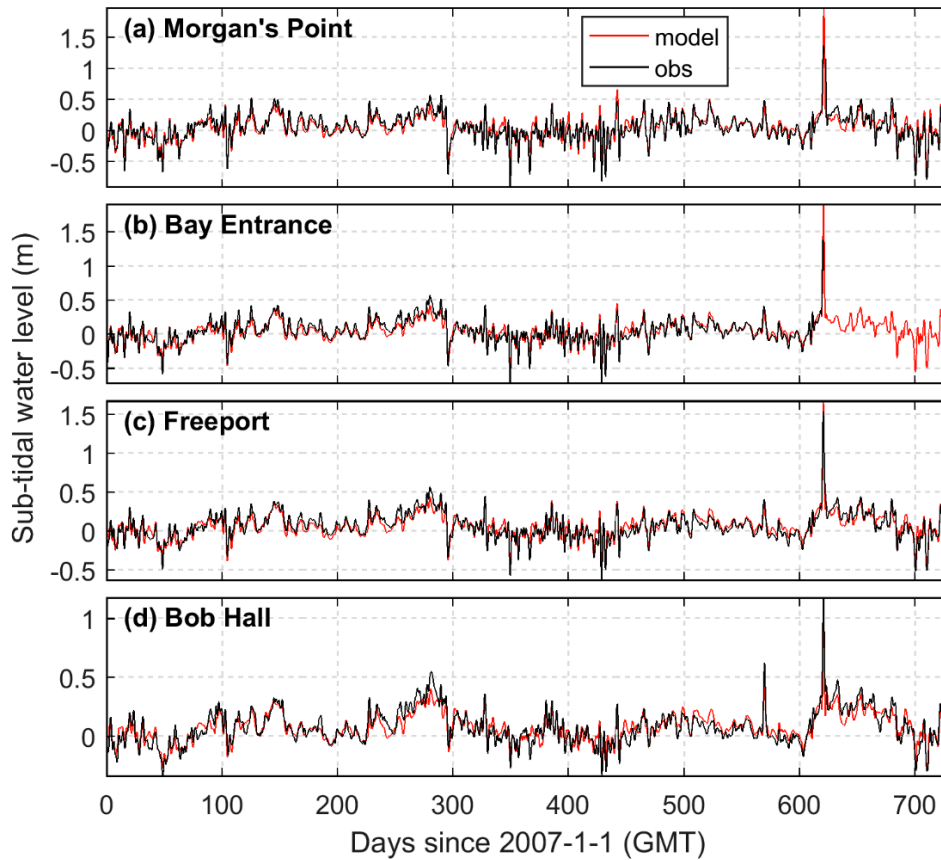
Figure 3: Subtidal surface elevation comparison between model (red line) and observation (black line) at NOAA tidal gauge stations (see Fig.2 for their locations).
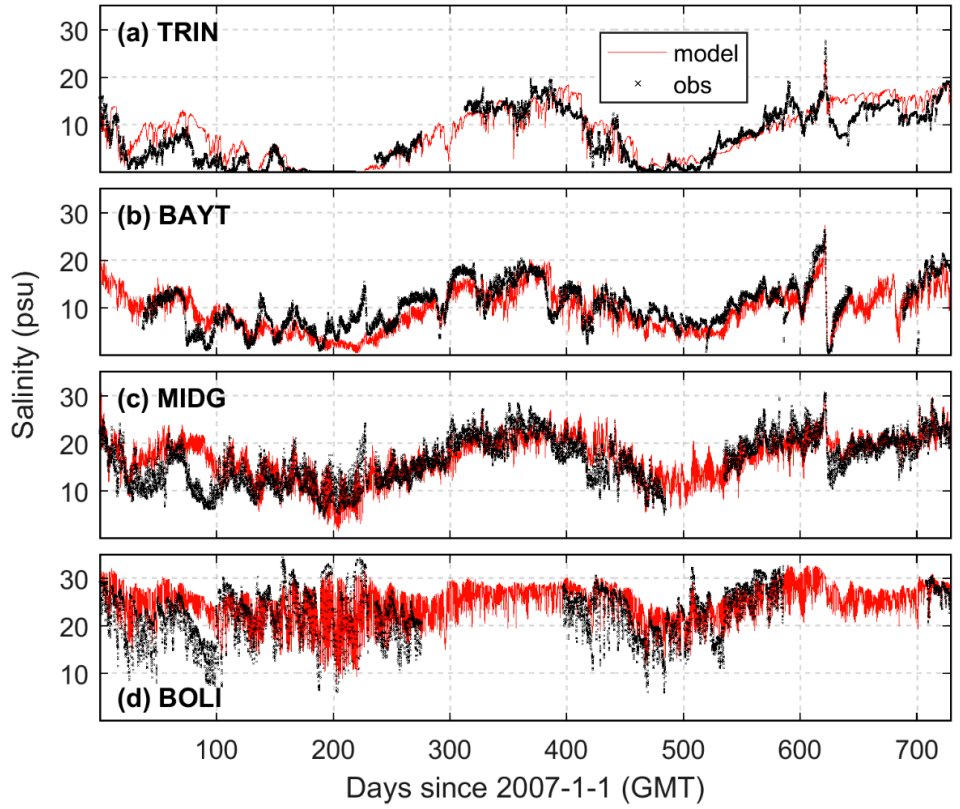
650

Figure 4: Salinity comparison between model (red line) and observation (black cross) at four TWDB stations (see Fig. 2 for their locations).
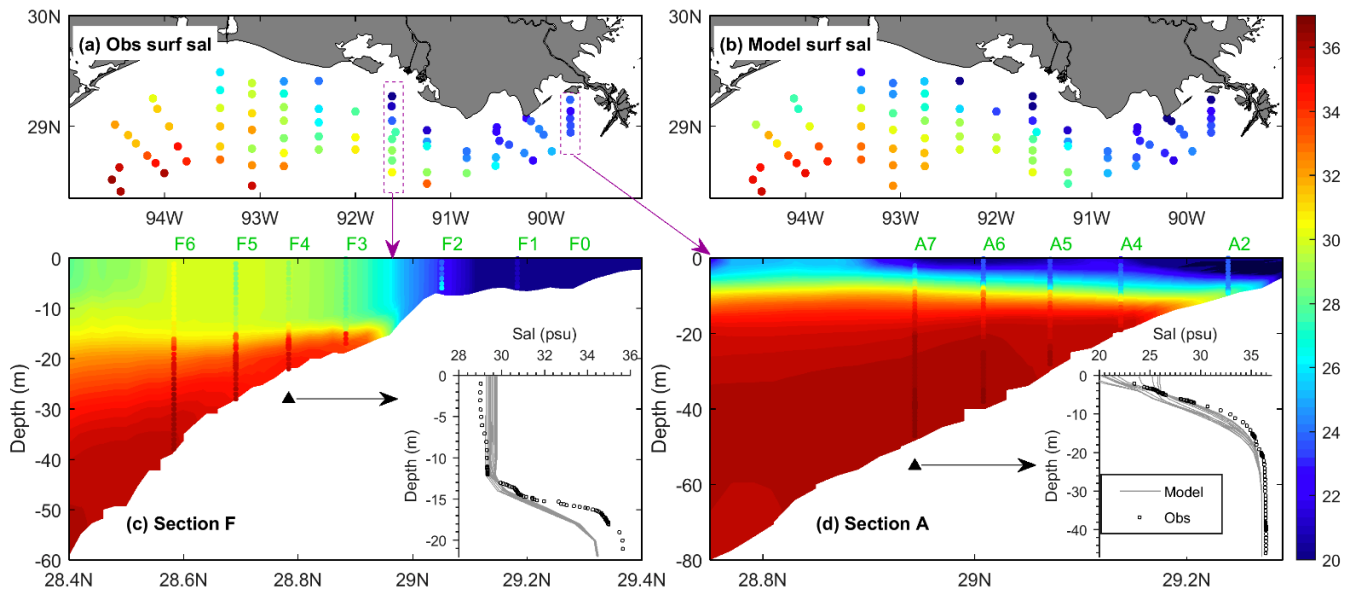
655

Figure 5: Salinity distribution at the Louisiana-Texas shelf from the shelf-wide survey on July 22-27, 2018: comparison of (a) observed and (b) modeled surface salinity and of the vertical profiles at two cross-shelf sections (c) F and (d) A. In (c) and (d), the colored dots indicate observed salinity while the filled colors indicate modeled salinity, and the insets compare the vertical profiles of salinity at the
660   selected stations of F4 and A7, respectively. The grey lines in the insets show the 12 modeled profiles over one day (the observation time ± 0.5 day).
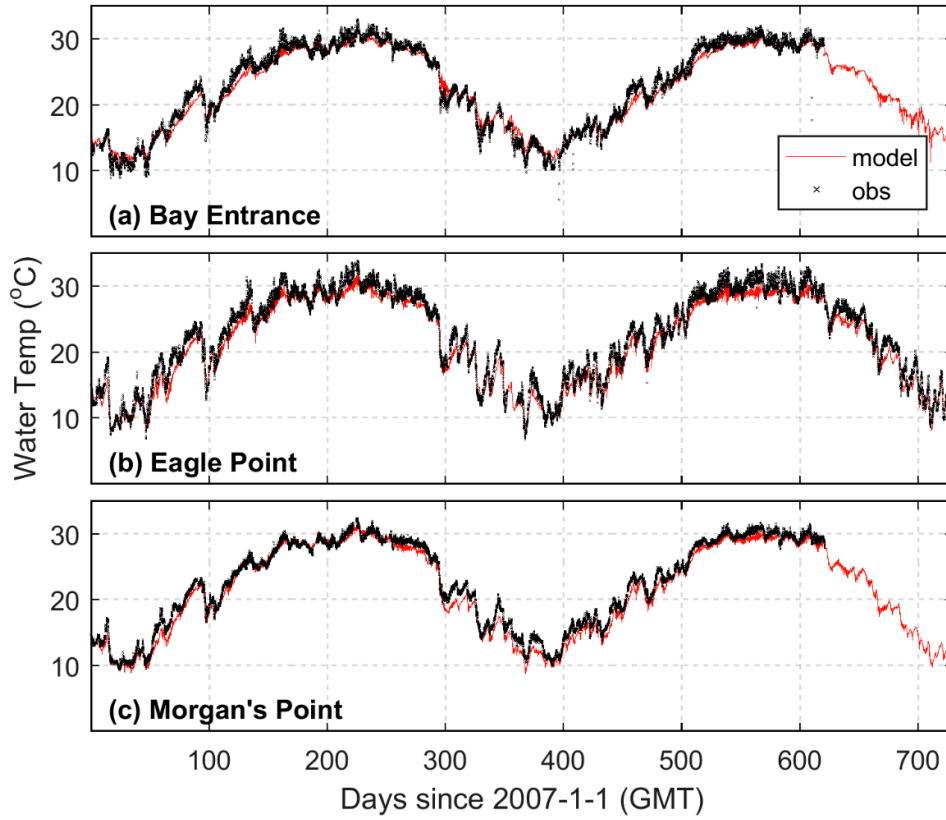
Figure 6: Temperature comparison between model (red line) and observation (black line) at three
NOAA stations (see Fig. 2 for their locations).
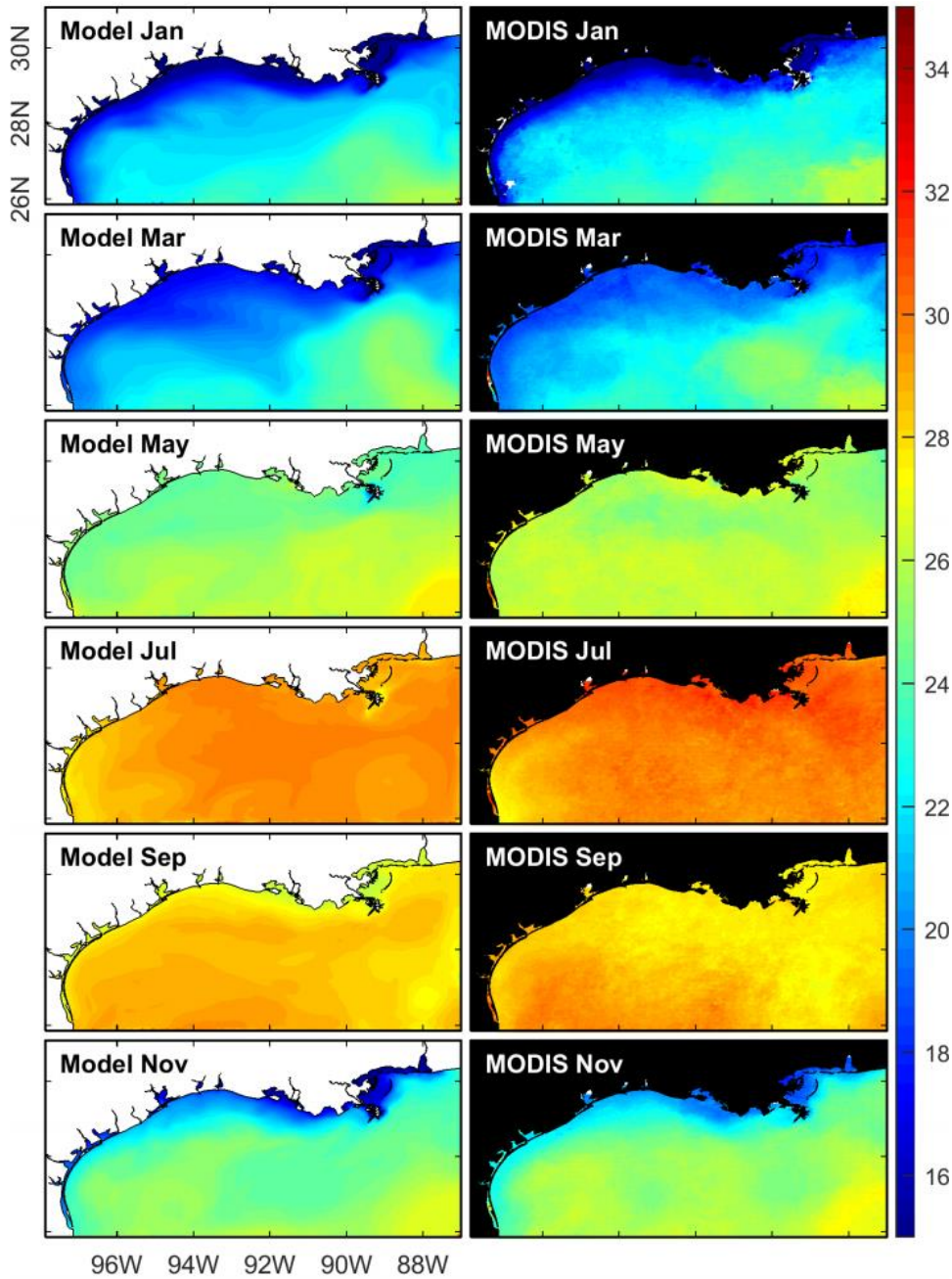
Figure 7: Temperature comparison (monthly average) between model (left panels) and MODIS satellite data (right panels) for selected months in 2008.

670
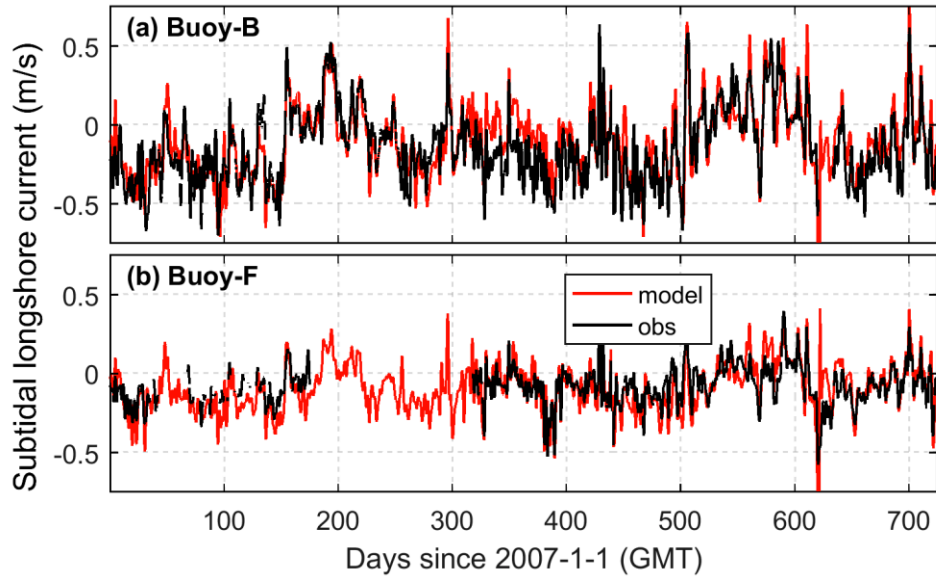
Figure 8: Comparison of the subtidal east-west surface shelf current between model (red line) and observation (black line) at two TABS buoys (see Fig. 2 for their locations).
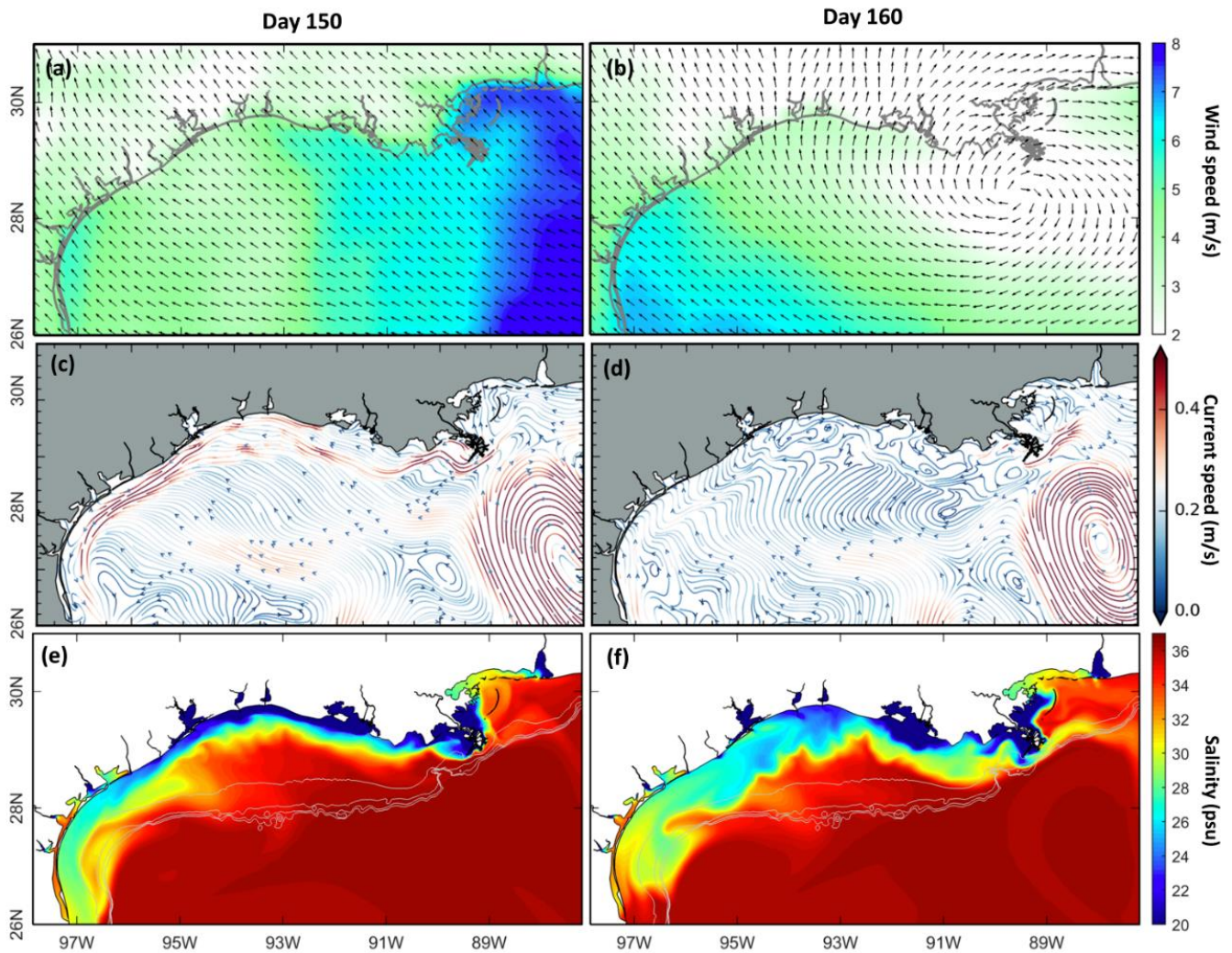
Figure 9: Comparison of the observed wind field and the modeled surface residual current and surface salinity on day 150 (May 31, 2007) and day 160 (June 10, 2017). The filled colors indicate the daily mean wind speed (a-b), speed of residual current (c-d) and salinity (e-f).
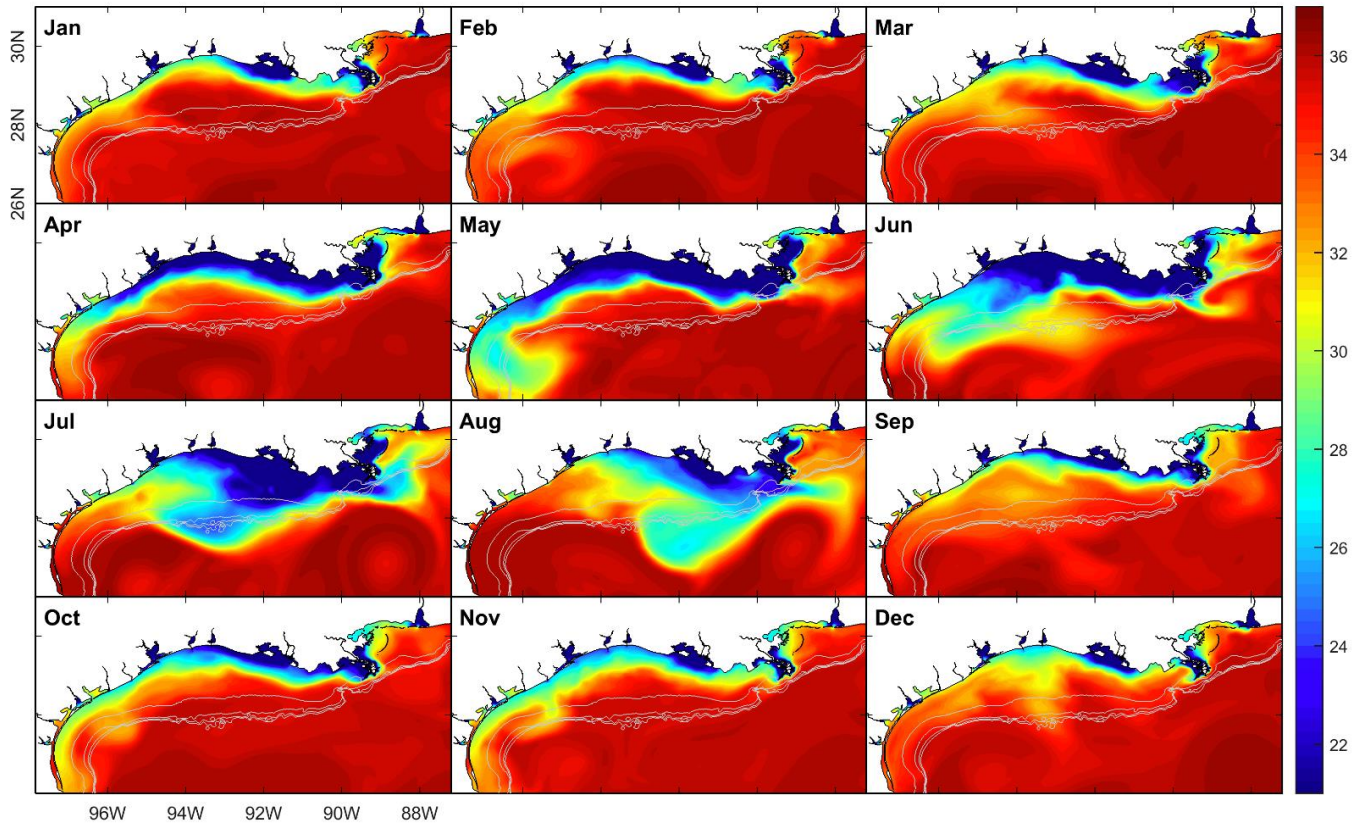
Figure 10: The modeled monthly mean surface salinity in 2008, with the grey contour lines denoting the depth contours of 50, 100, 150, 200 m.

685
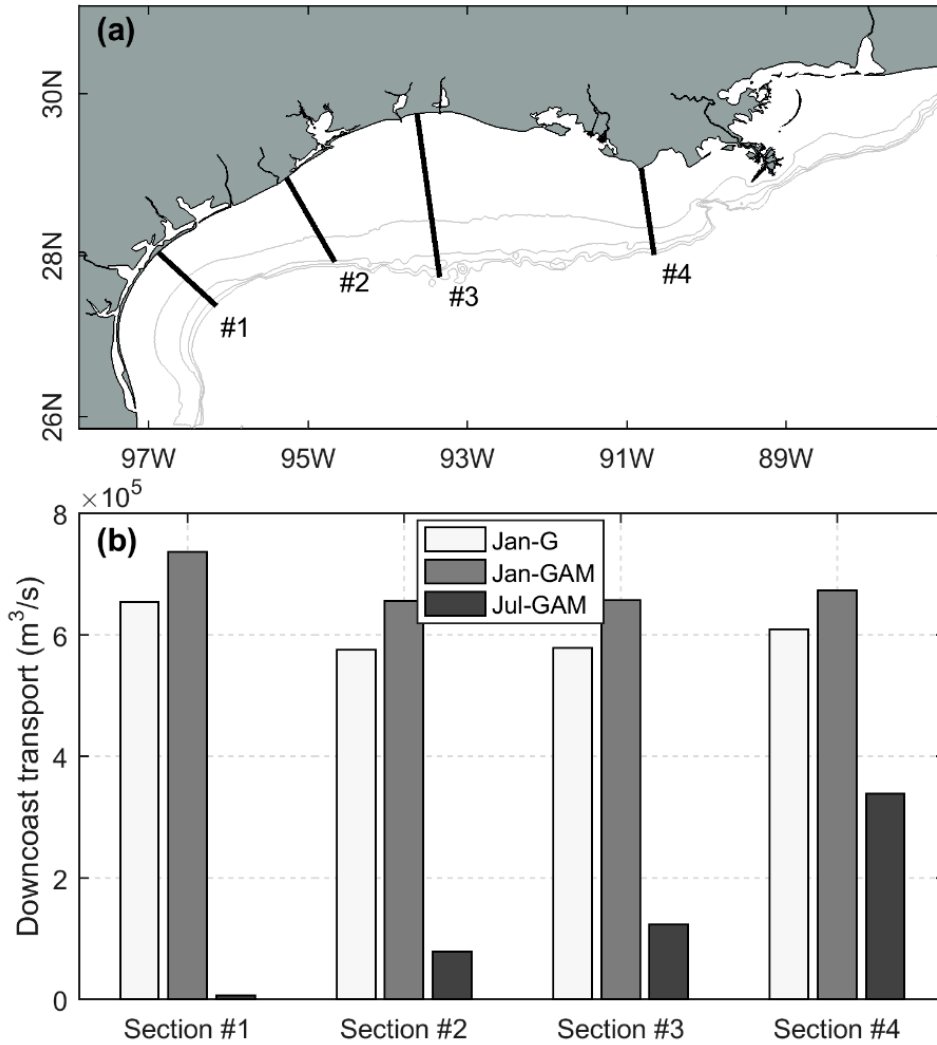
Figure 11: Downcoast longshore transport at four selected cross-shelf sections for three numerical experiments with constant long-term mean river discharges: river discharges into Galveston Bay only with January 2018 wind (Jan-G) and the MAR discharge as well as discharges into Galveston Bay with January 2018 wind (Jan-GAM) or July 2018 wind (Jul-GAM).
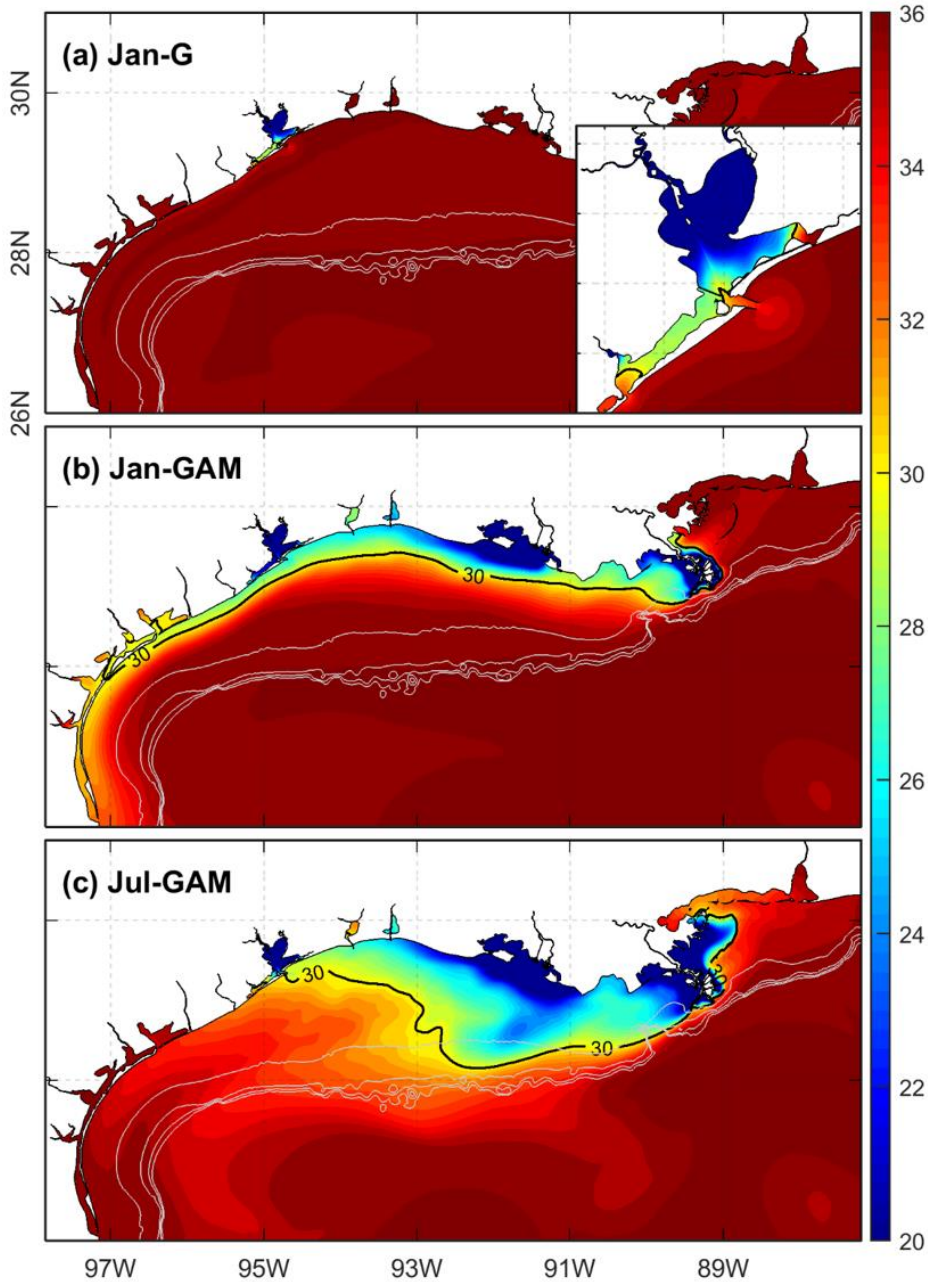
Figure 12: Surface salinity distributions, averaged over days 250-300, from three numerical experiments. Grey contour lines denote the depth contours for 50, 100, 150 and 200 m.

695
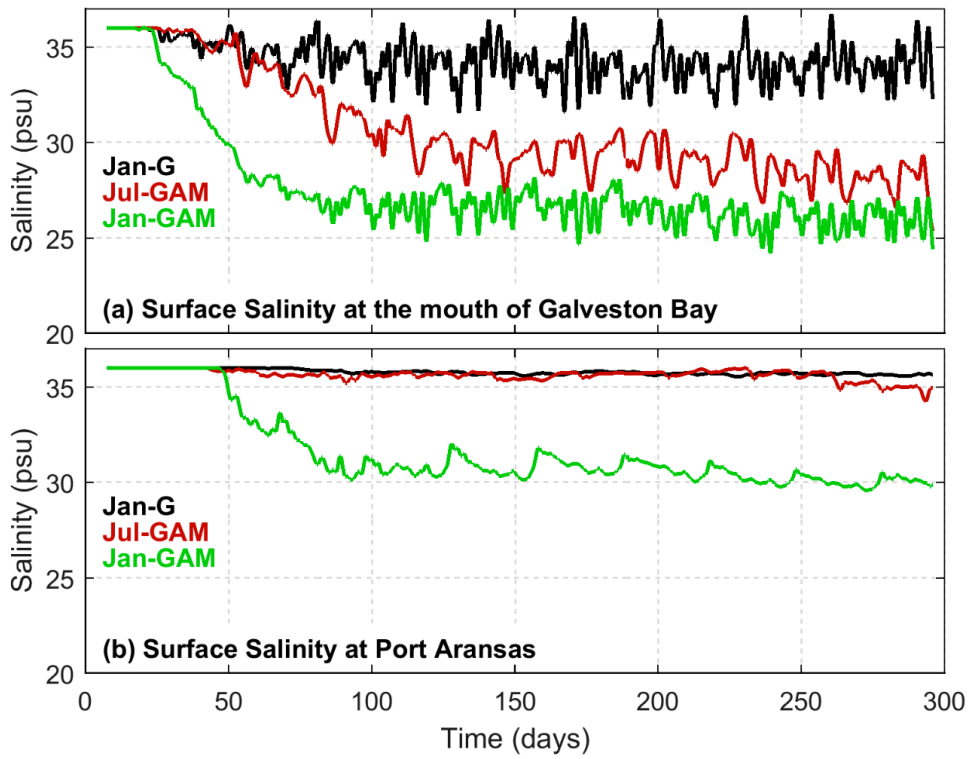
Figure 13: Subtidal surface salinity at the mouth of (a) Galveston Bay and (b) Aransas Bay for three numerical experiments.
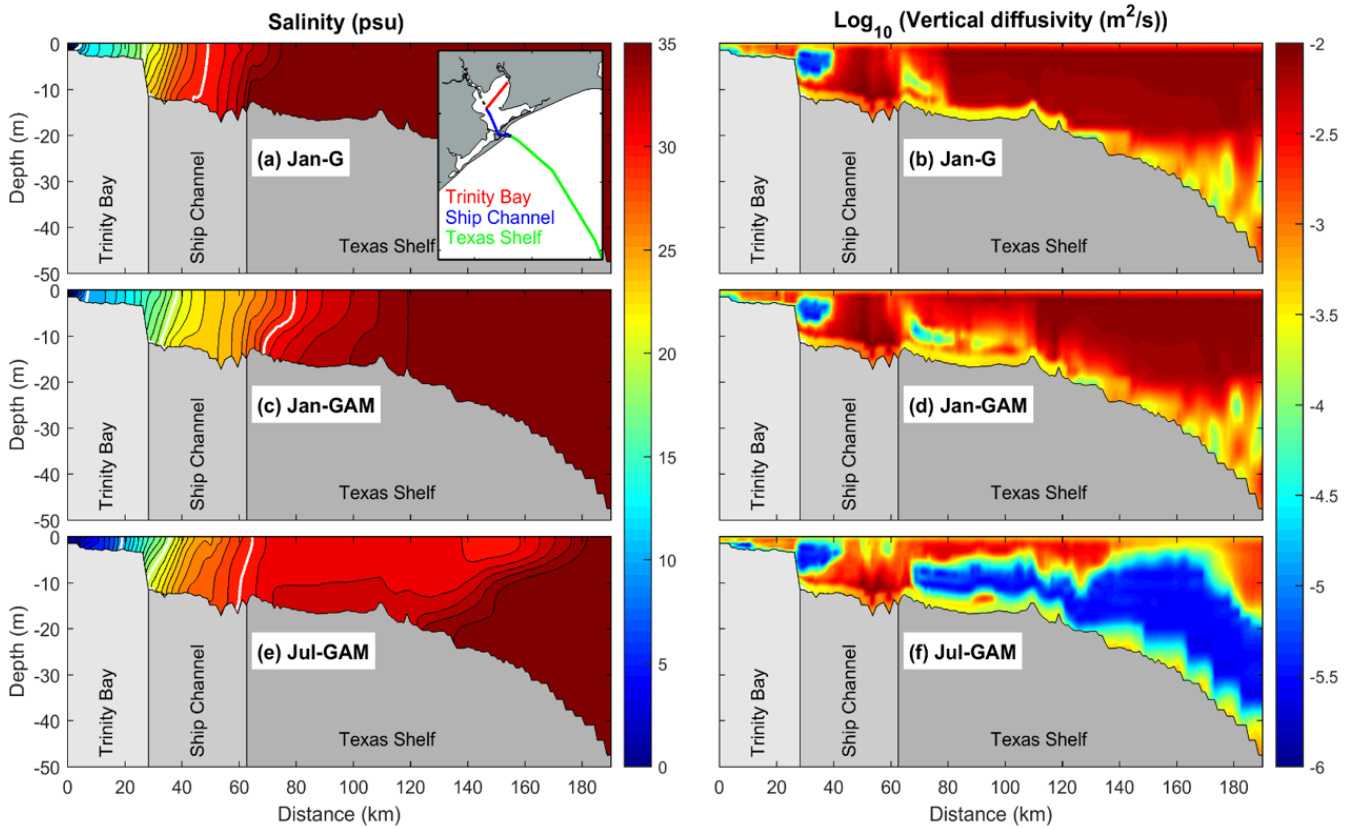
Figure 14: Salinity (left panels) and vertical diffusivity (right panels), averaged over days 250-300, from
705 three numerical experiments for the section through Trinity Bay, Galveston Bay ship channel, and Texas
shelf: see the inset in (a) for the section location. In (a), the bold white lines denote the salinity contours
of 10, 20, and 30 psu.
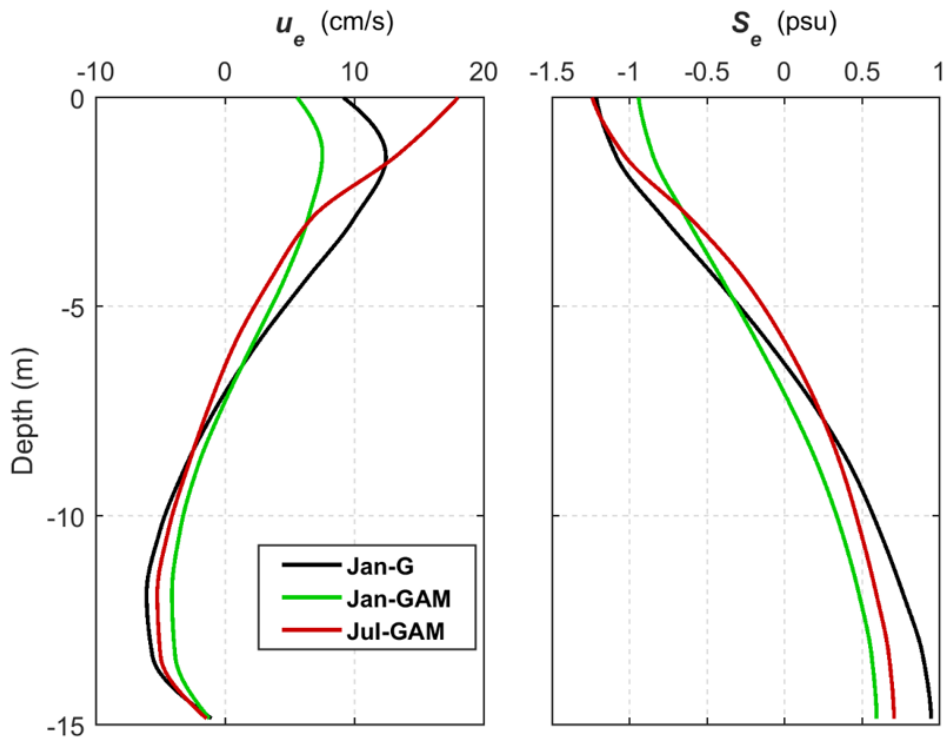
710   **Figure 15**: Vertical profiles of exchange flow (u_e) and salinity (S_e) at the deepest part of the Galveston Bay mouth, averaged over days 250-300, for three numerical experiments.